A Simulation Study on the Activation of Cardiac CaMKII δ-Isoform and Its Regulation by Phosphatases

Hiroaki Chiba,*† Natalie S. Schneider,* Satoshi Matsuoka,*‡ and Akinori Noma*‡
*Cell/Biodynamics Simulation Project, Kyoto University, Kyoto, Japan; †Pharmacology Laboratory, Mitsubishi Tanabe Pharma Corporation, Osaka, Japan; and ‡Department of Physiology and Biophysics, Graduate School of Medicine, Kyoto University, Kyoto, Japan

ABSTRACT Although the highly conserved Ca^{2+}/calmodulin-dependent protein kinase II (CaMKII) is known to play an essential role in cardiac myocytes, its involvement in the frequency-dependent acceleration of relaxation is still controversial. To investigate the functional significance of CaMKII autophosphorylation and its regulation by protein phosphatases (PPs) in heart, we developed a new mathematical model for the CaMKIIδ isoform. Due to better availability of experimental data, the model was first adjusted to the kinetics of the neuronal CaMKIIα isoform and then converted to a CaMKIIδ model by fitting to kinetic data of the δ isoform. Both models satisfactorily reproduced experimental data of the CaMKII-calmodulin interaction, the autophosphorylation rate, and the frequency dependence of activation. The level of autophosphorylated CaMKII cumulatively increased upon starting the Ca^{2+} stimulation at 3 Hz in the δ model. Variations in PP concentration remarkably affected the frequency-dependent activation of CaMKIIδ, suggesting that cellular PP activity plays a key role in adjusting CaMKII activation in heart. The inhibitory effect of PP was stronger for CaMKIIα compared to CaMKIIδ. Simulation results revealed a potential involvement of CaMKIIδ autophosphorylation in the frequency-dependent acceleration of relaxation at physiological heart rates and PP concentrations.

INTRODUCTION

With increasing heart rate, myocardial relaxation is accelerated to allow appropriate refilling of the ventricular cavity with the venous return (1,2). The Ca^{2+}/calmodulin-dependent protein kinase II (CaMKII) has been implicated in this autoregulation of frequency-dependent acceleration of relaxation (FDAR) (3–5). CaMKII is activated through the binding of Ca^{2+}-bound calmodulin (CaM) during the transient increase in the intracellular Ca^{2+} concentration ($[Ca^{2+}]_i$). In cardiac myocytes, activated CaMKII molecules phosphorylate many intracellular target proteins, including major components involved in excitation-contraction coupling (6,7), such as the sarcolemmal L-type Ca^{2+} channel, the ryanodine receptor, and the Ca^{2+} pump on the sarcoplasmic reticulum. With a rise in the frequency of the Ca^{2+} transient, the lifetime of activated CaMKII molecules is increased by intersubunit autophosphorylation, leading to an accumulation of the active CaMKII. Phosphorylated CaMKII maintains its catalytic activity even after the Ca^{2+} transient until it is inactivated by constitutive phosphatase activity. This was shown first for the brain-specific α and β isoforms of CaMKII and implicated in long-term potentiation, a mechanism playing a role in memory and learning (8,9). In heart, the predominant CaMKII isoform δ is found in two splice variants, δ_B localized to the nucleus and δ_C to the cytoplasm (10). Both variants were shown to undergo autophosphorylation (11). Autophosphorylation of CaMKII could potentiate the action of CaMKII during cyclic Ca^{2+} transients and thereby help to decode the stimulation frequency (12). However, the role of CaMKII and its autophosphorylation in the FDAR is still not well understood and is a subject of controversy (3,5,13,14). Furthermore, it has not yet been examined quantitatively how CaMKII activity is regulated by changes in heart rate.

Several computer models simulating CaMKII function have been developed based on in vitro experimental data, with the majority focusing on the neuronal CaMKII α and β isoforms (15–19). Although simple models for studying CaMKII activity in cardiac myocytes have been proposed, they are not directly based on experimental data on the δ isoform (20,21), nor do they consider deactivation of CaMKII by protein phosphatases (PPs) (22). It was experimentally demonstrated that the δ isoform has a higher affinity for CaM ($K_d = 33.5$ nM) compared to α ($K_d = 62.4$ nM) and a higher autophosphorylation rate, suggesting functional differences among the isoforms (22). Here, we introduce a novel CaMKII model that reflects the molecular properties of the δ isoform. This model achieves a good accordance with experimental data in vitro. The roles of CaMKII autophosphorylation and dephosphorylation by PPs in the frequency-dependent activation of CaMKII were demonstrated employing a cardiac Ca^{2+} transient model.

METHOD

Model structure

The CaMKII holoenzyme is a macromolecular complex consisting of two stacked ring-shaped hexamers. Binding of fully Ca^{2+}-bound CaM ($CaMCa_4$) to the autoinhibitory domain of CaMKII exposes the catalytic site, which is capable of phosphorylating a wide range of target proteins. In addition, an

Submitted July 28, 2007, and accepted for publication April 25, 2008.

Address reprint requests to Akinori Noma, Dept. of Physiology and Biophysics, Graduate School of Medicine, Kyoto University, Yoshida-konoe, Sakyo-ku, Kyoto, 606-8501, Japan. E-mail: noma@card.med.kyoto-u.ac.jp.

Satoshi Matsuoka's present address is Innovation Center for Immunoregulation Technologies and Drugs, Graduate School of Medicine, Kyoto University, Kyoto, 606-8501, Japan.

Editor: Jill Trewhella.

0006-3495/08/09/2139/11 $2.00

doi: 10.1529/biophysj.107.118505

activated CaMKII subunit is able to autophosphorylate neighboring subunits of the holoenzyme at Thr^{287}. A phosphorylated CaMKII subunit has a 1000-fold higher affinity for $CaMCa_4$ than a nonphosphorylated one. Furthermore, in the phosphorylated state, CaMKII shows partial activity even after dissociation of $CaMCa_4$. CaMKII is completely deactivated only after dephosphorylation by PPs (9).

CaM, a highly conserved protein, possesses at its C-terminal lobe two high-affinity Ca^{2+}-binding sites with a K_d of ~1–2 μM and at its N-terminal lobe two low-affinity sites with a K_d of ~2.6–13 μM, depending on experimental conditions (12,23,24). Since dissociation of Ca^{2+} from the C-terminal lobe is slow, the fraction of C- and N-terminal lobes occupied with Ca^{2+} might increase with increasing frequency of the Ca^{2+} transient. This mechanism may play an essential role in the activation of CaMKII. Therefore, we used the sequential four-step Ca^{2+} binding model described by Holmes (16) (CaM, CaMCa, $CaMCa_2$, $CaMCa_3$, $CaMCa_4$) (Fig. 1 *A*). This model includes cooperative Ca^{2+} binding within each lobe and assumes that the C-terminal Ca^{2+} binding sites are occupied before the N-terminal sites. The time-dependent changes of individual CaM states are determined as shown below:

$$CA1 = -k_1[Ca^{2+}][CaM] + k_{-1}[CaMCa] \quad (1)$$

$$CA2 = -k_2[Ca^{2+}][CaMCa] + k_{-2}[CaMCa_2] \quad (2)$$

$$CA3 = -k_3[Ca^{2+}][CaMCa_2] + k_{-3}[CaMCa_3] \quad (3)$$

$$CA4 = -k_4[Ca^{2+}][CaMCa_3] + k_{-4}[CaMCa_4] \quad (4)$$

$$d[CaMCa]/dt = -CA1 + CA2 \quad (5)$$

$$d[CaMCa_2]/dt = -CA2 + CA3 \quad (6)$$

$$d[CaMCa_3]/dt = -CA3 + CA4 \quad (7)$$

$$d[CaMCa_4]/dt = -CA4 \quad (8)$$

$$[CaM] = [CaM]_{total} - [CaMCa] - [CaMCa_2] - [CaMCa_3] - [CaMCa_4]. \quad (9)$$

A $[CaM]_{total}$ of 6 μM was used as reported for cardiac myocytes (12). Values for the rate constants (k_1, k_{-1}, k_2, k_{-2}, k_3, k_{-3}, k_4, and k_{-4}) were adapted from the original model (16), but adjusted to account for a temperature change from 25°C to 37°C (multiplied by 2.5; Table 1). The Hill coefficient (n_H) and $K_{0.5}$ for the $[Ca^{2+}]$-$CaMCa_4$ relationship are 1.9 and 26 μM, respectively. This relationship is slightly different from that measured in α-toxin permeabilized cells, which resulted in $n_H = 2.6$ and $K_d = 1$ μM (25). It should be noted that an accurate measurement of free $[CaMCa_4]$ in vivo is difficult, since about half of the CaM molecules are membrane bound and probably clustered (27) and many proteins compete for free $CaMCa_4$ molecules (25,28).

A four-state CaMKII model was developed, as shown in Fig. 1 *B*, with a nonactive state (CaMKII) and three active states, a $CaMCa_4$-bound state ($CaMKII\_CaMCa_4$), an autophosphorylated $CaMCa_4$-bound state ($CaMKIIP\_CaMCa_4$), and an autophosphorylated $CaMCa_4$-dissociated state (CaMKIIP). All active states are assumed to have the same activity. The rate A1 for the binding of $CaMCa_4$ to CaMKII is calculated with an association rate constant *k_asso* as follows:

$$A1 = k\_asso \times [CaMKII][CaMCa_4]. \quad (10)$$

For dissociation of $CaMCa_4$ from the $CaMKII\_CaMCa_4$ complex (rate A2 in Fig. 1 *B*), two pathways are assumed: In pathway 1, $CaMCa_4$ dissociates from $CaMKII\_CaMCa_4$ with a rate constant *k_disso*. In pathway 2, Ca^{2+} dissociates before separation of the $CaMKII\_CaMCa_4$ complex with a lumped rate constant *k_dissoCa*, which was determined by model fitting to be about one order faster than *k_disso* (Table 1). For the dissociation of Ca^{2+} from $CaMKII\_CaMCa_4$, a K_d value (*KmCaM*) is used as reported from experimental data (23). Assuming an instantaneous dissociation of Ca^{2+} from $CaMKII\_CaMCa_4$, step A2 is described as follows:

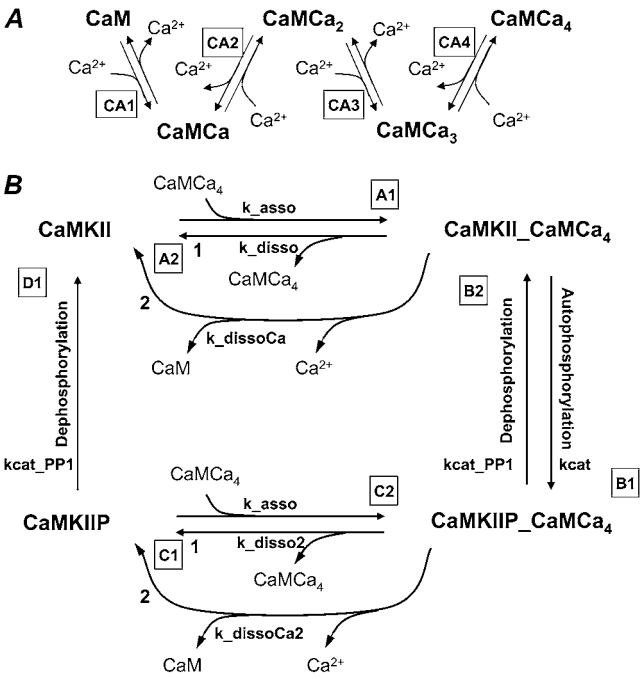

FIGURE 1 (*A*) Scheme of a CaM model (see Eqs. 1–9 for kinetic dynamics). (*B*) Scheme of a CaMKII model (see Eqs. 10–21 for kinetic dynamics). This model consists of one inactive state (CaMKII) and three active states ($CaMKII\_CaMCa_4$ ($CaMCa_4$ bound to CaMKII); $CaMKIIP\_CaMCa_4$ (phosphorylated $CaMKII\_CaMCa_4$); and CaMKIIP ($CaMCa_4$ dissociated from phosphorylated CaMKII dissociated from $CaMCa_4$)). For dissociation of $CaMCa_4$ from $CaMKII\_CaMCa_4$ (A2) or $CaMKIIP\_CaMCa_4$ (C1), two pathways are assumed, as indicated by numerals 1 and 2, respectively.

$$A2 = \left(k\_disso\left(1 - \frac{KmCaM2^3}{[Ca^{2+}]^3 + KmCaM2^3}\right) + k\_dissoCa\left(\frac{KmCaM2^3}{[Ca^{2+}]^3 + KmCaM2^3}\right)\right)[CaMKII\_CaMCa_4]. \quad (11)$$

The autophosphorylation of a CaMKII subunit is an intersubunit reaction within the same hexamer ring, with each subunit reacting only with neighboring subunits (9,29). For a given subunit, the probability (*P*) that either or both sides of a neighboring subunit are active is described by Eq. 12 using the probability that both sides are inactive.

$$P = 1 - \left([CaMKII]/[CaMKII]_{total}\right)^2. \quad (12)$$

Then the phosphorylation rate B1 from $CaMKII\_CaMCa_4$ to $CaMKIIP\_CaMCa_4$ is given as

$$B1 = kcat \times P\frac{[ATP]}{[ATP] + KmATP}[CaMKII\_CaMCa4], \quad (13)$$

where *kcat* is the rate constant, and *KmATP* is the Michaelis constant for the CaMKII-ATP complex.

Autophosphorylated CaMKII is dephosphorylated by several types of PPs (30,31), and 90% of PP activity in mammalian heart is mediated by PP1 and PP2A (32,33). Recently, PP1 was reported to dephosphorylate CaMKII in intact rat cardiac myocytes (14). In this study, only PP1 is considered. The dephosphorylation from $CaMKIIP\_CaMCa_4$ to $CaMKII\_CaMCa_4$ (Fig. 1 *B*, rate B2) is defined based on Michaelis-Menten kinetics, as shown below:

TABLE 1 List of parameter values

Parameter name	Value		Source
	α isoform	δ isoform	
$[CaM]_{total}$	6 μM		(12)
k_1	2.5 mM^{-1} ms^{-1}		(16)
k_{-1}, k_{-2}	0.05 ms^{-1}		(16)
k_2	88.25 mM^{-1} ms^{-1}		(16)
k_3	12.5 mM^{-1} ms^{-1}		(16)
k_{-3}, k_{-4}	1.25 ms^{-1}		(16)
k_4	250 mM^{-1} ms^{-1}		(16)
k_asso	2.1 mM^{-1} ms^{-1}		Model fit
k_disso	1.4×10^{-4} ms^{-1}	0.7×10^{-4} ms^{-1}	Model fit
k_dissoCa	1.9×10^{-3} ms^{-1}	0.95×10^{-3} ms^{-1}	Model fit
k_disso2	1.4×10^{-7} ms^{-1}	0.7×10^{-7} ms^{-1}	Model fit
k_dissoCa2	1.9×10^{-6} ms^{-1}	0.95×10^{-6} ms^{-1}	Model fit
KmCaM	3.0×10^{-5} mM		(23)
kcat (at 0°C)	1.0×10^{-5} ms^{-1}	6.0×10^{-5} ms^{-1}	Model fit
kcat (at 30°C)	3.0×10^{-4} ms^{-1}	1.8×10^{-3} ms^{-1}	(temperature
kcat (at 37°C)	9.0×10^{-4} ms^{-1}	5.4×10^{-3} ms^{-1}	change according to (29))
KmATP	19.1×10^{-3} mM		(22)
kcat_PP1	1.72×10^{-3} ms^{-1}		(34)
Km_PP1	11.0×10^{-3} mM		(34)

Note that only k_{cat} is temperature dependent.

$$B2 = kcat\_PP1\frac{[\text{CaMKIIP\_CaMCa}_4]}{[\text{CaMKIIP\_CaMCa}_4] + Km\_PP1}[\text{PP1}]. \quad (14)$$

Similarly, rate D1 for the dephosphorylation from CaMKIIP to CaMKII is calculated as

$$D1 = kcat\_PP1\frac{[\text{CaMKIIP}]}{[\text{CaMKIIP}] + Km\_PP1}[\text{PP1}], \quad (15)$$

where *Km_PP1* is the Michaelis constant for the PP1-CaMKII complex, and *kcat_PP1* is as determined in experiments (34).

The dissociation of $CaMCa_4$ from CaMKIIP_$CaMCa_4$ (rate C1) is calculated in the same way as for A2. However, the dissociation rate constants *k_disso2* and *k_dissoCa2* have a 1000-fold lower value compared to *k_disso* and *k_dissoCa*, respectively, because autophosphorylated CaMKII shows a 1000-fold higher affinity for $CaMCa_4$ (19).

$$\text{C1} = \left(\text{k\_disso2}\left(1 - \frac{\text{KmCaM2}^3}{[\text{Ca}^{2+}]^3 + \text{KmCaM2}^3}\right) + \text{k\_dissoCa2}\left(\frac{\text{KmCaM2}^3}{[\text{Ca}^{2+}]^3 + \text{KmCaM2}^3}\right)\right)[\text{CaMKIIP\_CaMCa}_4]. \quad (16)$$

The transition from CaMKIIP to CaMKIIP_$CaMCa_4$ (rate C2) is calculated in the same way as A1:

$$C2 = k\_asso \times [\text{CaMKIIP}][\text{CaMCa}_4]. \quad (17)$$

The time-dependent changes of individual CaMKII states are calculated as:

$$d[\text{CaMKII\_CaMCa4}]/dt = A1 - A2 - B1 + B2 \quad (18)$$

$$d[\text{CaMKIIP\_CaMCa}_4]/dt = B1 - B2 - C1 + C2 \quad (19)$$

$$d[\text{CaMKIIP}]/dt = C1 - C2 - D1 \quad (20)$$

$$[\text{CaMKII}] = [\text{CaMKII}]_{total} - [\text{CaMKII\_CaMCa}_4] - [\text{CaMKIIP\_CaMCa}_4] - [\text{CaMKIIP}]. \quad (21)$$

All parameter values employed in the models are shown in Table 1. Some parameters were chosen after fitting the model to results of in vitro experiments, as described below.

Since experimental data for the heart-predominant δ isoform are limited, a new kinetic model was first constructed for the brain-specific α isoform of CaMKII, for which experimental data obtained with different protocols are available. Then the δ isoform model was developed by modifying the parameter set of the α model according to the comparative experimental study carried out on the four isoforms of CaMKII by Gaertner et al. (22).

All experimental data referred to in this article were obtained from rat or mouse tissue. Since CaMKII shows a high sequence homology among species (35), the assumption might be justified that the same kinetic scheme and CaMKII activity are applicable to other species.

Generation of the Ca^{2+} transient

The hypothetical Ca^{2+} transient described by Negroni and Lascano (36) was used to test the frequency-dependent activation of CaMKII. Ca^{2+} release from sarcoplasmic reticulum is given by Q_{rel} and Ca^{2+} uptake by Q_{pump}:

$$Q_{pump} = K_P/\left(1 + \left(K_m/[Ca^{2+}]\right)^2\right) \quad (22)$$

$$Q_{rel} = Q_m(t/tp)^4 e^{4(1-t/tp)} + Q_{pumprest} \quad (23)$$

$$d[Ca^{2+}]/dt = Q_{rel} - Q_{pump}. \quad (24)$$

K_p (12 nM/ms) and K_m (0.1 μM) are Q_{pump} parameters. $Q_{pumprest}$ is a Q_{pump} at a resting $[Ca^{2+}]$ of 40 nM. Q_m (60 nM/ms) is the peak Q_{rel}, and *tp* (25 ms) is the time at Q_m.

The models were implemented in Java using the simBio package (37), software for cell simulation. Differential equations are solved using a Euler method with dynamically adjusted time steps.

Data analysis

To explore the degree of cooperativity in CaMKII activation, simulation results shown in Figs. 2 and 5 were fitted to the Hill equation (Eq. 25) by nonlinear regression analysis using SigmaPlot (Version 10; SPSS, Chicago, IL)

$$A = A_{max}[B]^{nH}/\left(K_{0.5}^{nH} + [B]^{nH}\right), \quad (25)$$

where A is the fraction of active CaMKII, with A_{max} expressing the maximum value; B is either CaM, free CaMKII, or Ca^{2+}; $K_{0.5}$ is $[B]$ at half-maximum; and n_H is the slope of the relationship (Hill coefficient). Fitted values are given with SE.

Since fitting the CaMKIIα model to different experimental conditions was done manually, a meaningful parameter identifiability analysis could not be applied. However, the simulation results were superimposed onto experimental data to assess the appropriate parameter fitting.

RESULTS

Analysis of $CaMCa_4$ binding to CaMKIIα

The dependency of CaMKIIα activation on $[CaMCa_4]$ (steps A1 and A2 of the model) was analyzed in the absence of ATP, i.e., no autophosphorylation. Fig. 2 *A* shows the experimental results described by De Koninck et al. (38) (*solid circles*) and Bradshaw et al. (34) (*open squares*), which were obtained by fixing the $[Ca^{2+}]$ and [CaMKII] and measuring the activation level of CaMKII in a quasi-steady state after addition of different [CaM] in vitro. With the assumption of a

1:1 binding of $CaMCa_4$ to CaMKII, i.e., $n_H = 1.0$, our CaMKIIα model reconstructed well these experimental results (Fig. 2 *A*, *solid line*). The $K_{0.5}$ (*k_disso*/*k_asso*) of 66.7 nM is within the range of various experimental $K_{0.5}$ values, such as 48 ± 6 nM (34) and 79 ± 8 nM (38) or the K_d value for $CaMCa_4$ binding (62.4 ± 25.1 nM) (22). The assumption of 1:1 binding, however, failed to simulate experimental results obtained by Gaertner et al. (22) (Fig. 2 *B*), who applied various [CaMKII]s to a solution containing fixed [Ca^{2+}] and [CaM], and plotted the CaM-bound fraction against free [CaMKII]. Gaertner et al. (22) obtained a steeper slope with $n_H = 1.9$ in their experiments, which they suggested was due to a positive cooperativity in the binding of $CaMCa_4$ to individual CaMKII molecules within the enzyme complex. However, the noncooperative binding of $CaMCa_4$ to CaMKII is further supported by experimental data from Bradshaw et al. (34), where the reaction of 0.2 μM CaMKII with 5 μM CaM was measured after adding 1–100 μM [Ca^{2+}] for 1 min (Fig. 2 *C*, *solid circles*). Simulation data obtained by applying the same experimental procedure yielded $n_H = 2.98 \pm 0.03$, which is in line with the experimental data. This high cooperativity results from cooperative binding of Ca^{2+} to CaM (Fig. 2 *C*, *solid line*).

Reconstruction of experiments measuring the CaMKIIα autophosphorylation rate

To examine the autophosphorylation rate, the dependency of the autophosphorylation level on either [CaM] or [Ca^{2+}] was analyzed in the presence of ATP. Fig. 3 shows a comparison of experimental findings with simulation results. Since the dephosphorylation step, B2 in the CaMKII model, is suppressed in the absence of phosphatase activity, the phosphorylation level reached after a given activation time is dependent on the overall autophosphorylation rate, which is determined by steps A1, A2, and B1 in the model. The solid line in Fig. 3 *A* indicates the sum of [CaMKIIP_$CaMCa_4$] and [CaMKIIP] obtained after a 15-s activation with different [CaM] at 0°C, according to the protocol by Gaertner et al. (22). Fig. 3 *B* shows the reconstruction of an experiment as performed by DeKoninck et al. (38), who measured the autophosphorylated fraction after 6 s at 30°C. Fig. 3 *C* shows a comparison of the simulation results with data from an experiment performed by Bradshaw et al. (34), who measured the autophosphorylation level 5 min after each applied [Ca^{2+}] at 0°C. The model parameters for the CaM-Ca^{2+} binding, and *k_asso*, *k_disso*, and *kcat* match well all experimental data tested above. The steeper slope in the relationship in Fig. 3 *C* is caused by the cooperative binding of Ca^{2+} to CaM. The saturation of the relationships in Fig. 3 is due to the saturation of the reaction rates of steps A and B at higher [CaM] or [Ca^{2+}], and not to completion of autophosphorylation. Thus, the saturation level is determined by the duration of the activation time unique to each experimental protocol. In the case of saturating high [Ca^{2+}], such as

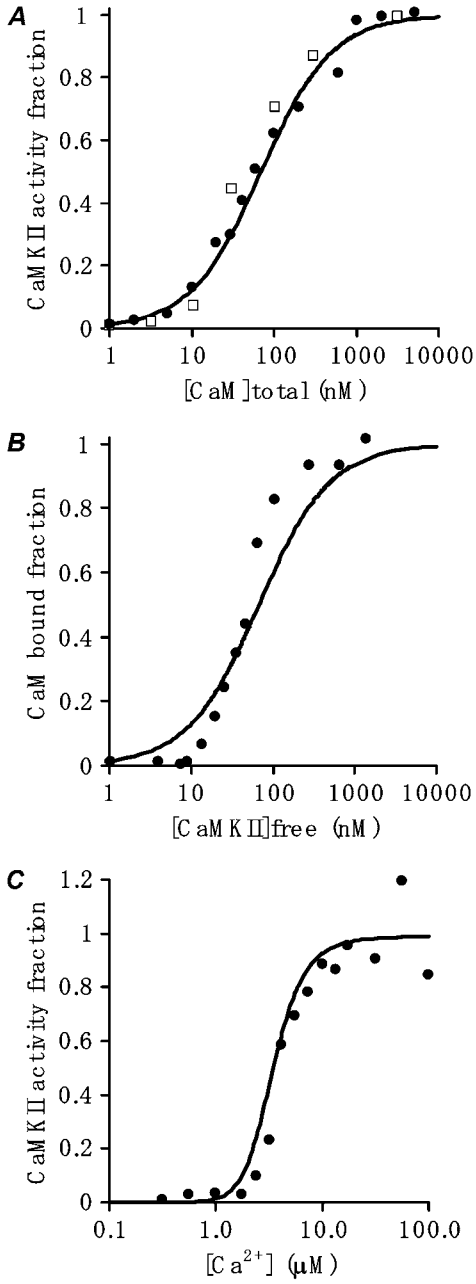

FIGURE 2 Quasi-steady-state activation of CaMKIIα by CaM. Simulations with the CaMKIIα model were carried out using in vitro experimental protocols. Solid circles and open squares represent experimental data, and solid lines the simulation results. (*A*) Experimental data are cited from Bradshaw et al. (34) (*squares*) and De Koninck and Shulman (38) (*circles*): In the presence of 500 μM Ca^{2+}, but the absence of ATP, 5 nM CaMKIIα was incubated with different [CaM] (1–10,000 nM) for 1 min. The ratio of [CaMKII_$CaMCa_4$] to $[CaMKII]_{total}$ is plotted against $[CaM]_{total}$ ($n_H = 1.02$; $K_{0.5} = 69.85 \pm 0.02$ nM). (*B*) Experimental data are cited from Gaertner et al. (22): In the presence of 500 μM Ca^{2+}, but the absence of ATP, 100 nM CaM was incubated with different [CaMKIIα] (1–10,000 nM) for 1 min. The ratio of [CaMKII_$CaMCa_4$] to $[CaM]_{total}$ is plotted against the free [CaMKII] ($n_H = 1.00$; $K_{0.5} = 67.46 \pm 0.00$ nM). (*C*) Experimental data are cited from Bradshaw et al. (34): In the absence of ATP and in the presence of different [Ca^{2+}] (0.1–100 μM), 0.2 μM CaMKII was incubated with 5 μM CaM for 1 min. The ratio of [CaMKII_$CaMCa_4$] to $[CaMKII]_{total}$ is plotted against [Ca^{2+}]; ($n_H = 2.98 \pm 0.03$; $K_{0.5} = 3.46 \pm 0.01$ μM).

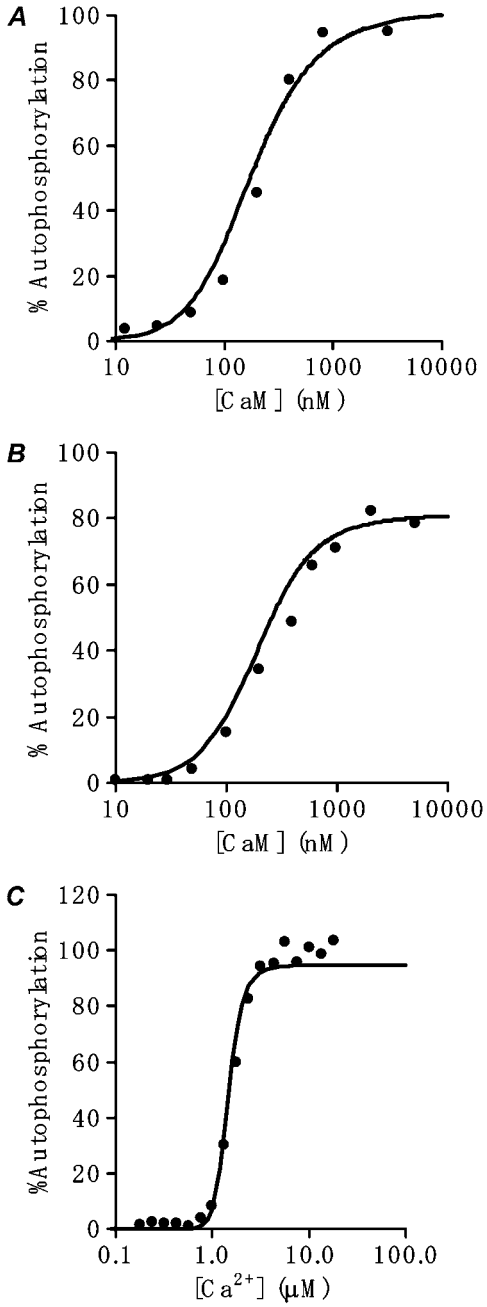

FIGURE 3 Relationship between the autophosphorylation level of CaMKIIα and [CaM] or [Ca^{2+}]. Solid circles represent the experimental data and solid lines the simulation results. (*A*) Experimental data are cited from Gaertner et al. (22): In the presence of 0.1 mM ATP and 500 μM Ca^{2+}, 62 nM CaMKIIα was incubated with different [CaM] (1–10,000 nM) for 15 s at 0°C. The ratio of ([CaMKIIP] + [CaMKIIP_$CaMCa_4$])/$[CaMKII]_{total}$) normalized to the maximum fraction is plotted against $[CaM]_{total}$. (*B*) Experimental data are cited from De Koninck and Shulman (38). In the presence of 0.25 mM ATP and 500 μM Ca^{2+}, 5 nM CaMKIIα was incubated with different [CaM] (1–10,000 nM) for 6 s at 30°C. The ratio of ([CaMKIIP] + [CaMKIIP_$CaMCa_4$])/$[CaMKII]_{total}$) is plotted against $[CaM]_{total}$. (*C*) Experimental data are cited from Bradshaw et al. (34): In the presence of 2 mM ATP and different [Ca^{2+}] (0.1–100 μM), 0.2 μM CaMKII was incubated with 50 μM CaM for 5 min at 0°C. The percentage of the autophosphorylated CaMKII fraction is plotted against [Ca^{2+}]. Different values of *kcat* were used for the simulations to adjust the temperature (see Table 1).

the 500 μM (*KmCaM* = 30 nM) used in the experiments shown in Fig. 3, *A* and *B* (Eq. 11), pathway 2 of step A2 is almost completely blocked. It should be noted that the fraction of CaMKIIP is a minor population in the sum of [CaMKIIP_$CaMCa_4$] and [CaMKIIP], because of the 1000-fold smaller *k_disso2* compared with *k_disso*.

Reconstruction of the frequency-dependent activation of CaMKIIα

The frequency-dependent activation of CaMKIIα was demonstrated by De Koninck et al. (38), who exposed CaMKII molecules immobilized on a membrane to a phosphorylation mixture containing Ca^{2+}, CaM, and ATP for a 200-ms duration at 1.0, 2.5, and 4.0 Hz. The CaMKII autophosphorylation level increased with time, as indicated in Fig. 4 (*symbols*), and the slope of this time-dependent increase was markedly accelerated with increasing phosphorylation frequency. As indicated by the solid lines in Fig. 4, the CaMKIIα model satisfactorily reconstructed these experimental data. During the time interval between the applications of the phosphorylation mixture, dissociation of $CaMCa_4$ from CaMKII_$CaMCa_4$ proceeded mainly along pathway 2 in the kinetic scheme in Fig. 1 *B*, in which Ca^{2+} dissociates from CaMKII_$CaMCa_4$ before the dissociation of CaM (23). When the application interval was shortened, at higher frequencies, the mean level of CaMKII_$CaMCa_4$ increased, which resulted in an accelerated accumulation of phosphorylated species. If hypothetical pathway 2 was eliminated from reaction step A2, the dissociation of $CaMCa_4$ from CaMKII_$CaMCa_4$ through pathway 1 was too slow during the stimulation interval, and the frequency dependence of the CaMKII autophosphorylation observed over the

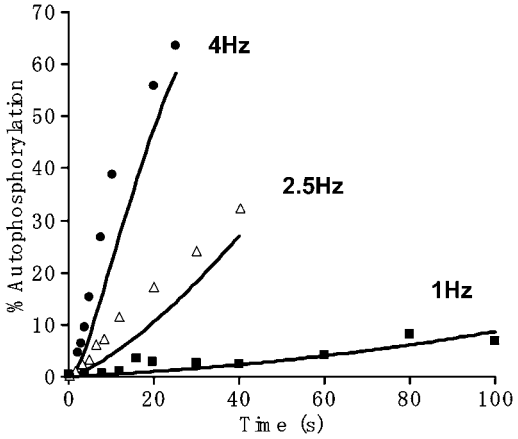

FIGURE 4 Frequency-dependent activation of CaMKIIα. Experimental data are cited from reference (38). The phosphorylation mixture (500 μM Ca^{2+}, 100 nM CaM, and 0.25 mM ATP) was applied to CaMKIIα for 200 ms at different frequencies; solid squares, open triangles, and solid circles represent 1, 2.5, and 4 Hz, respectively. During the interval of applying the phosphorylation mixture, [Ca^{2+}] was set at zero. Solid lines represent the simulation results.

range of ~1–4 Hz was highly reduced (data not shown). It should be noted that the involvement of pathway 2 is negligibly small under the experimental conditions used in Fig. 3, but becomes a major route when [Ca^{2+}] is low compared to the *KmCaM* of 30 nM (23) (see Eq. 11). The fact that Ca^{2+} was chelated using EGTA during the intervals in experiments by De Koninck et al. (38) validates the addition of pathway 2 in our model.

Parameter determination for the CaMKIIδ model

Gaertner et al. (22) found that the CaMKIIδ isoform exhibited a higher CaM affinity, specifically, $K_d = 33.5$ nM versus $K_d = 62.4$ nM, and a faster autophosphorylation compared to the CaMKIIα isoform. To convert the CaMKIIα model to a CaMKIIδ model with a minimum of modifications, the rate constants *k_disso*, *k_dissoCa*, *k_disso2*, and *k_dissoCa2* were decreased twofold and *kcat* was increased sixfold. Fig. 5 *A*, which corresponds to Fig. 2 *B* for the CaMKIIα isoform, compares the simulation results (*solid line*) with experimental data (*filled circles*) obtained with the CaMKIIδ isoform for the quasi-steady-state relationship between the free [CaMKII] and the $CaMCa_4$ bound fraction, [CaMKII_$CaMCa_4$]. Fig. 5 *B* represents the autophosphorylation level of CaMKIIδ accumulated after a 15-s application of different [CaM] (1–10,000 nM) at 0°C in the presence of 0.1 mM ATP and 500 μM Ca^{2+}, corresponding to Fig. 3 *A*, which shows the same relationship for CaMKIIα. The CaMKIIδ model obtained after the above-described changes of only five rate constants well matches experimental findings.

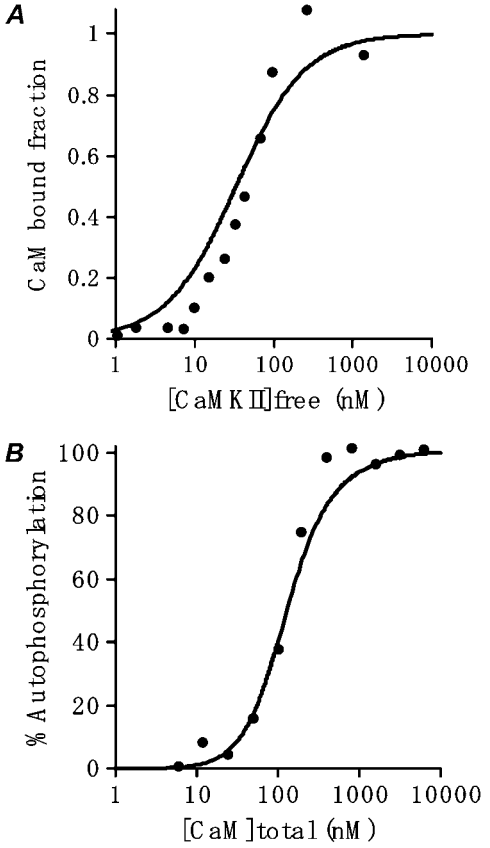

FIGURE 5 (*A*) Steady-state binding of CaM to CaMKIIδ and (*B*) CaMKIIδ autophosphorylation after a given activation time with [CaM]. Solid circles represent experimental data and solid lines the simulation results. Experimental data are cited from Gaertner et al. (22). (*A*) Experimental conditions used for the simulation are the same as described in Fig. 2 *B*; ($n_H = 1.0$; $K_{0.5} = 33.77 \pm 0.03$ nM). (*B*) Experimental conditions used for the simulation are the same as those described in Fig. 3 *A*.

Cumulative activation of CaMKIIδ by repetitive Ca^{2+}-transients

For the reconstructions of the experimental findings described above (Figs. 2–5), Ca^{2+} was either applied continuously or as repetitive 200-ms pulses. However, to investigate the potential role of CaMKII phosphorylation in the FDAR (3,5,13,14), it is important to use the ''physiological'' myocyte Ca^{2+} transient. The upper panels in Fig. 6 *A* show the cardiac Ca^{2+} transient (36), which was applied in the examination of the cumulative CaMKII activation as shown in Fig. 6 *B*. First, the time courses of [$CaMCa_2$] and [$CaMCa_4$] were calculated at stimulus frequencies of 3 and 5 Hz to examine whether active CaM accumulates with increasing stimulus frequency due to the slow dissociation of Ca^{2+} from the C-terminal lobe. As illustrated in the lower panels of Fig. 6 *A*, accumulation of active CaM is absent at 3 Hz, but a slight accumulation was detected at 5 Hz. This accumulation is due to a slight overlap of the Ca^{2+} tail with the next Ca^{2+} transient. On the contrary, the cumulative activation of CaMKII occurred progressively even at a stimulus frequency of 0.5 Hz (Fig. 6 *B*, *left panel*). The rapid rise of the [CaMKII_$CaMCa_4$] with a rise in the [Ca^{2+}] was followed by a relatively slow decay during each stimulus cycle. The phosphorylated fraction ([CaMKIIP_$CaMCa_4$]) increased steadily with time, eventually to 100%, since no phosphatase activity was provided in this simulation. Due to the slow relaxation during ''diastole'', the rate of [CaMKII_$CaMCa_4$] increase was markedly enhanced at the higher stimulus frequency of 3 Hz (Fig. 6 *B, right panel*). With time the [CaMKIIP_$CaMCa_4$] markedly increased at the expense of the [CaMKII_$CaMCa_4$]. It is suggested that the cumulative activation of CaMKIIδ is not attributable to the Ca^{2+} binding to CaM, but to the CaMKIIδ kinetics over the physiological range of the heart rate.

Regulation of activated CaMKIIδ through phosphatases

In vivo dephosphorylation by PPs affects the frequency-dependent activation of CaMKII. We first examined whether our CaMKIIα model could reproduce experimental data obtained for the neuronal CaMKIIα. The steady-state level of autophosphorylation was measured by Bradshaw et al. (34).

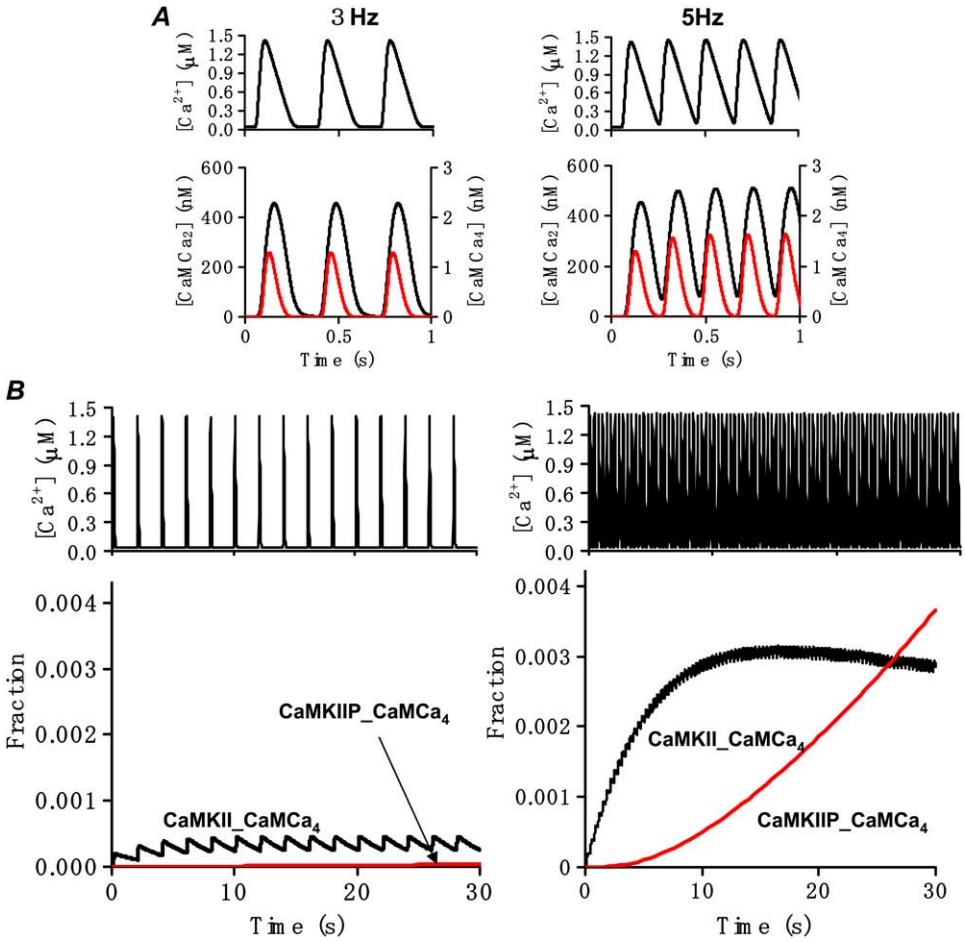

FIGURE 6 Cumulative activation of CaMKIIδ by Ca^{2+} transients in the absence of PPs. (*A*) Time courses for [$CaMCa_2$] (*lower panels*, *black lines*) and [$CaMCa_4$] (*red lines*) evoked by applying the Ca^{2+} transient of Negroni and Lascano (36) indicated in the upper panel at stimulus frequencies of 3 Hz (*left panel*) and 5 Hz (*right panel*). Stimulation was started at time zero after a long pause. (*B*) Simulation results obtained with the CaMKIIδ model activated with the Ca^{2+} transient at 0.5 Hz (*left panel*) or 3 Hz (*right panel*) at 37°C. Concentrations used are 5 mM [ATP], 6 μM [CaM], and 0.1 μM [CaMKIIδ]. Upper panels depict the Ca^{2+} transients, and lower panels show the time-dependent changes of the CaMKII_$CaMCa_4$ fraction (*black lines*) and the CaMKIIP_$CaMCa_4$ fraction (*red lines*). The changes in the CaMKIIP fraction were too small to be detected in these graphs.

The experimental findings are shown in Fig. 7 in comparison with simulation results obtained with essentially the same experimental protocol used in Fig. 3 *C*, but in the presence of 1.25 μM of PP1. The experimentally determined values of *kcat_PP1* and *Km_PP1* inserted in this CaMKIIα model could well reproduce these experimental data (34). Due to the lack of experimental data for the δ isoform, the same pair—*kcat_PP1* and *Km_PP1*—was used in the CaMKIIδ model to calculate this relation (Fig. 7, *red line*). The observed leftward shift of the [Ca^{2+}] dependency is due to the higher rates in A2 and B1, which were validated in Fig. 5.

In Fig. 8 *A*, the influence of PP1 on the frequency-dependent activation of CaMKIIδ was examined. To our knowledge, however, the cellular concentration of PPs has not been precisely measured, and region-specific variations in PP expression were found in the human heart (33). Therefore, we examined the opposing influence of PP1 on the autophosphorylation of CaMKII by systematically changing the [PP1] from 0.01 to 3 μM in the simulations. The steady-state values of the activated fraction, given by ($[CaMKII]_{total}$ − [CaMKII])/$[CaMKII]_{total}$, are plotted against the frequency (Fig. 8 *A*). At a low [PP1] of 0.01 μM, the activated fraction of CaMKIIδ is highly frequency-dependent, ranging from 14% at 0.5 Hz to 96% at 5 Hz, displaying a hyperbolic relationship. With increasing [PP1], the activation-frequency curve changes to a sigmoidal shape over the medium range of [PP1] and to an exponential relation for high phosphatase levels. At a [PP1] of 3 μM, CaMKIIδ autophosphorylation was almost completely suppressed.

To demonstrate functional differences between the CaMKII isoforms, the same simulation protocol was applied to the CaMKIIα model. As shown in Fig. 8 *B*, CaMKIIα activation was much more sensitive to [PP1]. A [PP1] of 0.1 μM could almost suppress the activation. These results are due to the lower affinity of CaMKIIα for CaM and its slower autophosphorylation rate.

The relationship shown in Fig. 8 *A* suggests a role of PPs in the dynamic adjustment of CaMKIIδ activity over the physiological range of the heart rate. For example, in guinea pig heart, with a physiological frequency range of 3–6 Hz, a [PP1] of 0.1–0.3 μM might play a role, whereas in the human heart, with a rate of 1–3 Hz, a much lower [PP1] of 0.01–0.03 μM might be appropriate.

DISCUSSION

To clarify the dynamic regulation of the CaMKII activation, especially through variation of both the heart rate and the

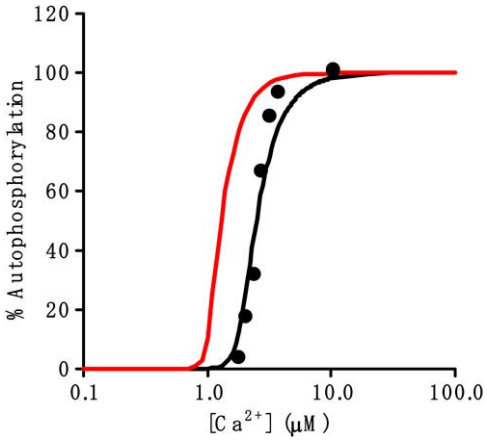

FIGURE 7 Ca^{2+}-mediated activation of CaMKIIα and CaMKIIδ in the presence of PP1. Solid circles represent experimental data and solid lines the simulation results for CaMKIIα (*black*) and CaMKIIδ (*red*). Experimental data are cited from Bradshaw et al. (34). In the presence of 2 mM ATP and different [Ca^{2+}] (0.1–100 μM), 1 μM CaMKII and 1.25 μM PP1 were incubated with 5 μM CaM at 0°C. The steady-state value of the autophosphorylated CaMKII fraction is plotted against [Ca^{2+}].

concentration of PPs, a novel and simple four-state CaMKIIδ model was developed that includes autophosphorylation and dephosphorylation by PP1. Although several cardiac CaMKII models were reported, they were not directly fitted to experimental data of the δ isoform (20,21) or did not include the deactivation of CaMKII by dephosphorylation (22). Both models, CaMKIIα and CaMKIIδ, used in this study could well reproduce experimental findings regarding the steady-state dose-response relationships for activation by $CaMCa_4$ (Figs. 2 and 5 *A*), and the time-dependent accumulation of activated CaMKII fraction (Figs. 3 and 5 *B*). Simulations for the frequency-dependent activation of CaMKIIα induced by a repetitive pulse-like application of the phosphorylation mixture interrupted by a Ca^{2+}-free medium strongly supports the existence of pathway 2 of step A2 in the kinetic scheme (Fig. 1), where Ca^{2+} dissociates before CaM from $CaMCa_4$-bound CaMKII. The PP1 regulation of the frequency-dependent accumulation of activated CaMKII was clarified. In particular, PP1 within a physiological concentration range (0.01–0.1 μM) provides a dynamic way to regulate the frequency-dependent activation of CaMKIIδ, and the heart rate variations are well covered. Our simulation results suggest that different phosphatase activities might be involved in frequency-dependent regulation of CaMKII activity, adjusting the activation level of CaMKII to the various physiological heart rates found for different species.

Significance of CaMKII autophosphorylation in the cardiac FDAR

Total concentrations of CaM, PP1, and CaMKII greatly affect simulation results, as exemplified by varying the concentration of PP1 in Fig. 8. In this study, protein con-

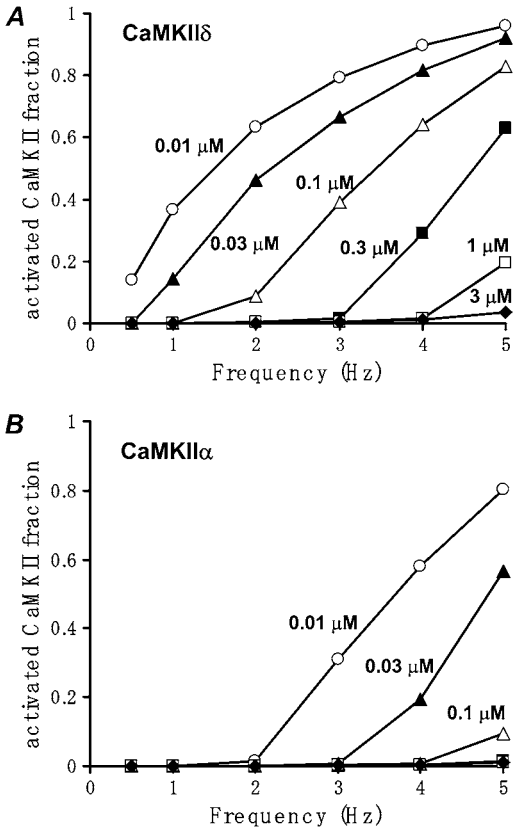

FIGURE 8 Effects of [PP1] variation on the frequency-dependent activation of CaMKII. The cardiac Ca^{2+} transient, shown in Fig. 6 *A* was applied at different frequencies (0.5, 1, 2, 3, 4, and 5 Hz) to the CaMKIIδ (*A*) and the CaMKIIα model (*B*). The steady-state values of ($[CaMKII]_{total} - [CaMKII]$)/$[CaMKII]_{total}$ are plotted against the frequency of the Ca^{2+} transient. The simulations were performed in the presence of 5 mM ATP, 6 μM CaM, and a total [CaMKII] of 0.1 μM for different [PP1] (0, 0.01, 0.03, 0.1, 0.3, 1, and 3 μM) at 37°C.

centrations were chosen that represent the level expected for cardiac myocytes. A $[CaM]_{total}$ of 6 μM is in accordance with an experimental measurement in cardiac myocytes (12). Although it is difficult to directly measure [PP1] and [CaMKII] in experiments, we estimated a [PP1] based on experimental values of PP1 activity/total cellular protein, A_p, of 1.07 units/mg (39), and protein concentration, $[P]_{cell}$, of 37.5 mg/ml (40) measured in cardiac myocytes. Using a PP1-specific activity, A_s, of 13,300 units/mg and the PP1 molecular weight ($M_{PP1} = 36{,}000$), [PP1] was determined as 0.084 μM using the equation

$$[\mathrm{PP1}] = \frac{10^6 \times [P]_{cell} \times A_p}{A_s \times M_{pp1}}. \quad (26)$$

The [CaMKII] was determined, in the same way used for [PP1], to be 0.12 μM, using CaMKII activity of 4 units/mg measured in cardiac myocytes (41), the same protein concentration as above (40), a CaMKII specific activity of 21,100 units/mg, and a CaMKII molecular weight of 58,000.

The combination of 0.1 μM [CaMKII], 0.1 μM [PP1], and 6 μM $[CaM]_{total}$ in Fig. 8 *A* well reconciled the apparent dissociation of FDAR and protein phosphorylation by CaMKII suggested by Huke and Bers (14). They found no change in the amount of phosphorylated CaMKII after 2-Hz pacing for 5 min in rat cardiac myocytes. A rise of CaMKII autophosphorylation was observed only after a strong inhibition of PP1 at the 2-Hz pacing. They suggested that CaMKII has no role in FDAR. Our simulation results, presented in Fig. 8, are in roughly good agreement with their experimental results. In particular, in the presence of a physiological [PP1] of 0.1 μM, the fraction of activated CaMKII is negligibly small at 2-Hz stimulation, but gains significance progressively with decreasing PP1 activity, which would correspond to an experimental blocking of PPs. However, it is interesting to note that the simulation predicts that CaMKII is indeed a feasible candidate for regulating FDAR over the physiological heart rate (~240–400 min^{-1}, or 4–7 Hz) in rat heart. At these higher frequencies, dynamic changes in the autophosphorylation of CaMKII are apparent in Fig. 8 even at high [PP1] such as 1 μM. We conclude that CaMKII is capable of mediating cardiac FDAR, with CaMKII autophosphorylation playing a role.

Functional differences between CaMKIIα and CaMKIIδ

The structural and enzymatic differences among the α, β, γ, and δ CaMKII isoforms were extensively studied in vitro, and their differences were reported to be small (22). However, it was suggested that subtle changes among these isoforms might result in drastic differences in the activation dynamics under various cellular environments (22). For converting the α isoform model to the CaMKIIδ model based on experimental data, a twofold decrease in the CaM affinity and a sixfold increase in the autophosphorylation rate were required. To estimate the physiological impact of these differences, simulations were performed with both models using the same cardiac myocyte specific Ca^{2+} transient only for comparison, although neuronal Ca^{2+} transients are different (16) in both time course and peak magnitude from Ca^{2+} transients in cardiac myocytes. According to our simulation results (Fig. 8 *B*), CaMKIIα autophosphorylation was suppressed at all frequencies tested by a [PP1] of 0.1 μM, which is close to our estimated cellular [PP1] in cardiac myocytes. This is in strong contrast to the results in Fig. 8 *A*, where CaMKIIδ was strongly activated at higher frequencies.

CaMKIIα is accumulated at the postsynaptic density in neurons and involved in long-term potentiation, which is induced by high stimulation frequencies (~30 Hz) (8,9,41). Therefore, lower frequencies, such as 5 Hz, used in the preent simulations described here do not seem sufficient to activate CaMKIIα, especially in the presence of PPs. This clearly shows that CaMKII isoforms are adapted to meet the conditions in their respective cellular environment.

Model limitations

As our proposed model is a simple one, it exhibits limitations. For all three active states considered in the model (CaMKII_$CaMCa_4$, CaMKIIP_$CaMCa_4$, and CaMKIIP) the same autophosphorylation activity was assumed. This is different than the general assumption that some CaMKII states exhibit only partial activity, in particular, CaMKIIP (19). However, since the fraction of CaMKIIP is quite small compared to those of the other two active states, a variation of the autophosphorylation activity for different states might not remarkably influence our conclusions. Moreover, CaMKIIα autophosphorylated at Thr^{286} was shown to undergo further autophosphorylation at Thr^{305}/Thr^{306} after dissociation of CaM, known as secondary or inhibitory autophosphorylation. In this state, sometimes called the capped state (19), CaMKII still exhibits some autonomous activity, but it cannot regain full activity through $CaMCa_4$ binding since these threonine residues reside in the CaM binding site. It has been reported that inhibitory autophosphorylation plays an important role in synaptic metaplasticity (42). Since, to our knowledge, it is not known whether secondary autophosphorylation occurs in cardiac myocytes, a capped state was not considered in our model.

Experimental data for the kinetic properties of CaMKIIδ are still very limited. Therefore, our model may have to be modified in the future according to newly obtained experimental results, especially concerning the localization of CaM, PPs, and CaMKII molecules within the cell, as well as their local concentrations. In this study, [PP1] and [CaMKII] were estimated based on average, probably cytoplasmic, concentrations within the cell (Eq. 26). Any variation in the Ca^{2+} affinity of the N-terminal lobe of CaM largely affects reaction step A1 by varying the [$CaMCa_4$] (Fig. 1). K_d measurements for Ca^{2+} binding to the N-terminal lobe of CaM are variable, ranging from 2.6 to 13 μM depending on experimental conditions (12,23,24). It should be noted that the simulation study presented here is useful in designing new experimental studies despite the above-stated limitations of the model.

Importance of CaMKII-PP1 regulation in heart disease

Although CaMKII autophosphorylation might be insignificant in the normal heart, due to strong control by phosphatases, an almost threefold increase in CaMKII activity was found in patients with end-stage dilated cardiomyopathy (43). Furthermore, in mice in which pressure overload was induced by aortic constriction, Zhang et al. found that the expression of $CaMKII\delta_C$ was upregulated and the kinase activity was increased due to autophosphorylation (44). The same group found, in addition, that transgenic mice overexpressing $CaMKII\delta_C$ developed a dilated cardiomyopathy. In an immunoprecipitation compared to wild-type mice, a

greater amount of the enzyme was associated with the ryanodine receptor, a CaMKII target, resulting in a high phosphorylation of the receptor and, subsequently, a strongly altered Ca^{2+} homeostasis (45), whereas PP1 and PP2A protein levels were unaltered (44). Moreover, in transgenic mice overexpressing the phosphatase calcineurin which resulted in a severe cardiomyopathy, CaMKII activity was also found to be increased (46). The above experimental findings clearly show that in cardiac myocytes, CaMKII and its PPs need to be highly regulated, and that a tiny disturbance of this balance could result in heart disease. Future work will incorporate the CaMKIIδ model presented here in a comprehensive cardiac myocyte model to analyze these complex mechanisms.

This study was supported by the Leading Project for Biosimulation from the Ministry of Education, Culture, Sports, Science and Technology of Japan. We thank the members of the Leading Project for continuous and useful discussions.

REFERENCES

1. Kassiri, Z. 2000. Rate-dependent changes of twitch force duration in rat cardiac trabeculae: a property of the contractile system. *J. Physiol.* 524:221–231.
2. Endoh, M. 2004. Force–frequency relationship in intact mammalian ventricular myocardium: physiological and pathophysiological relevance. *Eur. J. Pharmacol.* 500:73–86.
3. Bassani, R. A., A. Mattiazzi, and D. M. Bers. 1995. CaMKII is responsible for activity-dependent acceleration of relaxation in rat ventricular myocytes. *Am. J. Physiol.* 268:H703–H712.
4. Picht, E., J. DeSantiago, S. Huke, M. A. Kaetzel, J. R. Dedman, and D. M. Bers. 2007. CaMKII inhibition targeted to the sarcoplasmic reticulum inhibits frequency-dependent acceleration of relaxation and Ca^{2+} current facilitation. *J. Mol. Cell. Cardiol.* 42:196–205.
5. DeSantiago, J., L. S. Maier, and D. M. Bers. 2002. Frequency-dependent acceleration of relaxation in the heart depends on CaMKII, but not phospholamban. *J. Mol. Cell. Cardiol.* 34:975–984.
6. Maier, L. S., and D. M. Bers. 2007. Role of Ca^{2+}/calmodulin-dependent protein kinase CaMK in excitation-contraction coupling in the heart. *Cardiovasc. Res.* 73:631–640.
7. Zhang, T., S. Miyamoto, and J. H. Brown. 2004. Cardiac myocyte calcium and calcium/calmodulin-dependent protein kinase II: friends or foes? *Recent Prog. Horm. Res.* 59:141–168.
8. Lisman, J., H. Schulman, and H. Cline. 2002. The molecular basis of CaMKII function in synaptic and behavioural memory. *Nat. Rev. Neurosci.* 3:175–190.
9. Hudmon, A., and H. Schulman. 2002. Structure-function of the multifunctional Ca^{2+}/calmodulin-dependent protein kinase II. *Biochem. J.* 364:593–611.
10. Srinivasan, M., C. F. Edman, and H. Schulman. 1994. Alternative splicing introduces a nuclear localization signal that targets multifunctional CaM kinase to the nucleus. *J. Cell Biol.* 126:839–852.
11. Edman, C. F., and H. Schulman. 1994. Identification and characterization of δ_B-CaM kinase and δ_C-CaM kinase from rat heart, two new multifunctional Ca^{2+}/calmodulin-dependent protein kinase isoforms. *Biochim. Biophys. Acta.* 1221:89–101.
12. Maier, L. S., and D. M. Bers. 2002. Calcium, calmodulin, and calcium-calmodulin kinase II: heartbeat to heartbeat and beyond. *J. Mol. Cell. Cardiol.* 34:919–939.
13. Valverde, C. A., C. Mundina-Weilenmann, M. Said, P. Ferrero, L. Vittone, M. Salas, J. Palomeque, M. V. Petroff, and A. Mattiazzi. 2005. Frequency-dependent acceleration of relaxation in mammalian heart: a property not relying on phospholamban and SERCA2a phosphorylation. *J. Physiol.* 562:801–813.
14. Huke, S., and D. M. Bers. 2007. Temporal dissociation of frequency-dependent acceleration of relaxation and protein phosphorylation by CaMKII. *J. Mol. Cell. Cardiol.* 42:590–599.
15. Coomber, C. J. 1998. Site-selective autophosphorylation of Ca^{2+}/calmodulin-dependent protein kinase II as a synaptic encoding mechanism. *Neural Comput.* 10:1653–1678.
16. Holmes, W. R. 2000. Models of calmodulin trapping and CaM kinase II activation in a dendritic spine. *J. Comput. Neurosci.* 8:65–85.
17. Zhabotinsky, A. M. 2000. Bistability in the Ca^{2+}/calmodulin-dependent protein kinase-phosphatase system. *Biophys. J.* 79:2211–2221.
18. Kubota, Y., and J. M. Bower. 2001. Transient versus asymptotic dynamics of CaM kinase II: possible roles of phosphatase. *J. Comput. Neurosci.* 11:263–279.
19. Dupont, G., G. Houart, and P. De Koninck. 2003. Sensitivity of CaM kinase II to the frequency of Ca^{2+} oscillations: a simple model. *Cell Calcium.* 34:485–497.
20. Hund, T. J., and Y. Rudy. 2004. Rate dependence and regulation of action potential and calcium transient in a canine cardiac ventricular cell model. *Circulation.* 110:3168–3174.
21. Iribe, G., P. Kohl, and D. Noble. 2006. Modulatory effect of calmodulin-dependent kinase II CaMKII on sarcoplasmic reticulum Ca^{2+} handling and interval-force relations: a modelling study. *Philos. Transact. A Math. Phys. Eng. Sci.* 364:1107–1133.
22. Gaertner, T. R., S. J. Kolodziej, D. Wang, R. Kobayashi, J. M. Koomen, J. K. Stoops, and M. N. Waxham. 2004. Comparative analyses of the three-dimensional structures and enzymatic properties of α, β, γ and δ isoforms of Ca^{2+}-calmodulin-dependent protein kinase II. *J. Biol. Chem.* 279:12484–12494.
23. Peersen, O. B., T. S. Madsen, and J. J. Falke. 1997. Intermolecular tuning of calmodulin by target peptides and proteins: differential effects on Ca^{2+} binding and implications for kinase activation. *Protein Sci.* 6:794–807.
24. Johnson, J. D., C. Snyder, M. Walsh, and M. Flynn. 1996. Effects of myosin light chain kinase and peptides on Ca^{2+} exchange with the N- and C-terminal Ca^{2+} binding sites of calmodulin. *J. Biol. Chem.* 271:761–767.
25. Persechini, A., and B. Cronk. 1999. The relationship between the free concentrations of Ca^{2+} and Ca^{2+}-calmodulin in intact cells. *J. Biol. Chem.* 274:6827–6830.
26. Tran, Q. K., D. J. Black, and A. Persechini. 2003. Intracellular coupling via limiting calmodulin. *J. Biol. Chem.* 278:24247–24250.
27. Teruel, M. N., W. Chen, A. Persechini, and T. Meyer. 2000. Differential codes for free Ca^{2+}-calmodulin signals in nucleus and cytosol. *Curr. Biol.* 10:86–94.
28. Persechini, A., and P. M. Stemmer. 2002. Calmodulin is a limiting factor in the cell. *Trends Cardiovasc. Med.* 12:32–37.
29. Bradshaw, J. M., A. Hudmon, and H. Schulman. 2002. Chemical quenched flow kinetic studies indicate an intraholoenzyme autophosphorylation mechanism for Ca^{2+}/calmodulin-dependent protein kinase II. *J. Biol. Chem.* 277:20991–20998.
30. Ishida, A., Y. Shigeri, T. Taniguchi, and I. Kameshita. 2003. Protein phosphatases that regulate multifunctional Ca^{2+}/calmodulin-dependent protein kinases: from biochemistry to pharmacology. *Pharmacol. Ther.* 100:291–305.
31. Herzig, S., and J. Neumann. 2000. Effects of serine/threonine protein phosphatases on ion channels in excitable membranes. *Physiol. Rev.* 80:173–210.
32. El-Armouche, A., A. Bednorz, T. Pamminger, D. Ditz, M. Didie, D. Dobrev, and T. Eschenhagen. 2006. Role of calcineurin and protein phosphatase-2A in the regulation of phosphatase inhibitor-1 in cardiac myocytes. *Biochem. Biophys. Res. Commun.* 346:700–706.
33. Luss, H., O. Klein-Wiele, P. Boknik, S. Herzig, J. Knapp, B. Linck, F. U. Muller, H. H. Scheld, C. Schmid, W. Schmitz, and J. Neumann.

2000. Regional expression of protein phosphatase type 1 and 2A catalytic subunit isoforms in the human heart. *J. Mol. Cell. Cardiol.* 32:2349–2359.

34. Bradshaw, J. M., Y. Kubota, T. Meyer, and H. Schulman. 2003. An ultrasensitive Ca^{2+}/calmodulin-dependent protein kinase II-protein phosphatase 1 switch facilitates specificity in postsynaptic calcium signaling. *Proc. Natl. Acad. Sci. USA.* 100:10512–10517.
35. Tombes, R. M., M. O. Faison, and J. M. Turbeville. 2003. Organization and evolution of multifunctional Ca^{2+}/CaM-dependent protein kinase genes. *Gene.* 322:17–31.
36. Negroni, J. A., and E. C. Lascano. 1996. A cardiac muscle model relating sarcomere dynamics to calcium kinetics. *J. Mol. Cell. Cardiol.* 28:915–929.
37. Sarai, N., S. Matsuoka, and A. Noma. 2006. simBio: a Java package for the development of detailed cell models. *Prog. Biophys. Mol. Biol.* 90:360–377.
38. De Koninck, P., and H. Schulman. 1998. Sensitivity of CaM kinase II to the frequency of Ca^{2+} oscillations. *Science.* 279:227–230.
39. Yamada, M., Y. Ikeda, M. Yano, K. Yoshimura, S. Nishino, H. Aoyama, L. Wang, H. Aoki, and M. Matsuzaki. 2006. Inhibition of protein phosphatase 1 by inhibitor-2 gene delivery ameliorates heart failure progression in genetic cardiomyopathy. *FASEB J.* 20:1197–1199.
40. Merten, K. E., Y. Jiang, W. Feng, and Y. J. Kang. 2006. Calcineurin activation is not necessary for doxorubicin-induced hypertrophy in H9c2 embryonic rat cardiac cells: involvement of the phosphoinositide 3-kinase-Akt pathway. *J. Pharmacol. Exp. Ther.* 319:934–940.
41. Johnston, D., B. R. Christie, A. Frick, R. Gray, D. A. Hoffman, L. K. Schexnayder, S. Watanabe, and L. L. Yuan. 2003. Active dendrites, potassium channels and synaptic plasticity. *Philos. Trans. R. Soc. Lond. B Biol. Sci.* 358:667–674.
42. Zhang, L., T. Kirschstein, B. Sommersberg, M. Merkens, D. Manahan-Vaughan, Y. Elgersma, and H. Beck. 2005. Hippocampal synaptic metaplasticity requires inhibitory autophosphorylation of Ca^{2+}/calmodulin-dependent kinase II. *J. Neurosci.* 25:7697–7707.
43. Kirchhefer, U., W. Schmitz, H. Scholz, and J. Neumann. 1999. Activity of cAMP-dependent protein kinase and Ca^{2+}/calmodulin-dependent protein kinase in failing and nonfailing human hearts. *Cardiovasc. Res.* 42:254–261.
44. Zhang, T., L. S. Maier, N. D. Dalton, S. Miyamoto, J. Jr. Ross, D. M. Bers, and J. H. Brown. 2003. The δ_C isoform of CaMKII is activated in cardiac hypertrophy and induces dilated cardiomyopathy and heart failure. *Circ. Res.* 92:912–919.
45. Maier, L. S., T. Zhang, L. Chen, J. DeSantiago, J. H. Brown, and D. M. Bers. 2003. Transgenic CaMKIIδc overexpression uniquely alters cardiac myocyte Ca^{2+} handling: reduced SR Ca^{2+} load and activated SR Ca^{2+} release. *Circ. Res.* 92:904–911.
46. Khoo, M. S., J. Li, M. V. Singh, Y. Yang, P. Kannankeril, Y. Wu, C. E. Grueter, X. Guan, C. V. Oddis, R. Zhang, L. Mendes, G. Ni, E. C. Madu, J. Yang, M. Bass, R. J. Gomez, B. E. Wadzinski, E. N. Olson, R. J. Colbran, and M. E. Anderson. 2006. Death, cardiac dysfunction, and arrhythmias are increased by calmodulin kinase II in calcineurin cardiomyopathy. *Circulation.* 114:1352–1359.